RSC Advances

PAPER

View Article Online
View Journal | View Issue

Cite this: *RSC Adv.*, 2017, **7**, 12085

Received 10th December 2016
Accepted 8th February 2017

DOI: 10.1039/c6ra28015c

rsc.li/rsc-advances

Ultrathin Ag nanoparticles anchored on urchin-like $WO_3 \cdot 0.33H_2O$ for enhanced photocatalytic performance†

Haoqi Ren,[a] Xufeng Gou[b] and Qing Yang*[b]

Ultrathin Ag nanoparticles anchored on urchin-like $WO_3 \cdot 0.33H_2O$ can be successfully achieved by a novel and facile self-catalytic reduction approach, and displayed a better solar-driven photocatalytic performance than that of the individual $WO_3 \cdot 0.33H_2O$.

As an important n-type semiconductor, tungsten oxide hydrate ($WO_3 \cdot 0.33H_2O$) has been demonstrated to be a promising material for the photocatalytic degradation of organic dyes.[1–3] In the past few years, many efforts have been employed into the shape-controlled synthesis of $WO_3 \cdot 0.33H_2O$ crystals. Although morphological $WO_3 \cdot 0.33H_2O$, such as nanoplates, nanorods, and hierarchical architectures, has been successfully synthesized,[4–8] individual $WO_3 \cdot 0.33H_2O$ is not an efficient photocatalyst because of its weak light-harvesting and relatively low conduction band (CB) level.[9,10]

So far, two general strategies have been developed to improve the photocatalytic activity of $WO_3 \cdot 0.33H_2O$. One is the controllable synthesis of $WO_3 \cdot 0.33H_2O$ with high-active building blocks.[4–8] The other one is the modification of $WO_3 \cdot 0.33H_2O$, such as doping and hybridizing.[11,12] Especially, a heterogeneous junction originating from the intimate contact of a metal with a semiconductor, is very useful for improving the photocatalytic performance of the pristine semiconductor, because it can effectively limit the recombination of photogenerated electrons and holes.[1] Consequently, the combination of the above two strategies is a perspective pathway to effectively improve the photocatalytic activity of $WO_3 \cdot 0.33H_2O$. However, it has been rarely reported on the metal/$WO_3 \cdot 0.33H_2O$ for enhanced photocatalytic activity. Therefore, to precisely control the structure of hybrid metal/$WO_3 \cdot 0.33H_2O$ composite, and thorough understanding of the formation and photocatalytic mechanisms are imperative.

Herein, we report a novel and facile self-catalytic reduction approach for the achievement of ultrathin silver (Ag) nanoparticles anchored on urchin-like $WO_3 \cdot 0.33H_2O$ assembly of rod-like building blocks. When evaluated the photocatalytic performance, the as-prepared Ag/$WO_3 \cdot 0.33H_2O$ composite exhibited a better photodegradation of Rhodamine B (RhB) than that of the individual $WO_3 \cdot 0.33H_2O$ under simulated solar light irradiation. The preparation of this novel Ag/$WO_3 \cdot 0.33H_2O$ hybridizing architecture could provide a good opportunity to understand the foundational significance of metal nanoparticle for improving the photocatalytic activity of semiconductor.

Fig. 1a is the powder X-ray diffraction (XRD) pattern of the as-synthesized Ag/$WO_3 \cdot 0.33H_2O$ composite. The main diffraction peaks can be indexed by the orthorhombic $WO_3 \cdot 0.33H_2O$ (JCPDS card no. 72-0199, and the thermogravimetric analysis (TGA) can be used for further determining the stoichiometry of the hydrated water in the oxide, see Fig. S2†). Moreover, it can be seen that there are slight diffraction peaks at 38.1°, 44.3°, 64.4° and 77.5° (marked by rhomboic symbol), respectively, which are indexed by the cubic Ag (JCPDS card no. 87-0719). Electron energy dispersive X-ray (EDX) analysis can also be used to characterize the chemical composition, and the tungsten, silver and oxygen element are detected (see Fig. 1b), further indicating the formation of Ag/$WO_3 \cdot 0.33H_2O$ composite.

Fig. 2 shows the scanning electron microscope (SEM) images of the as-synthesized Ag/$WO_3 \cdot 0.33H_2O$ composite with different magnifications. A low-magnification SEM image (see Fig. 2a)

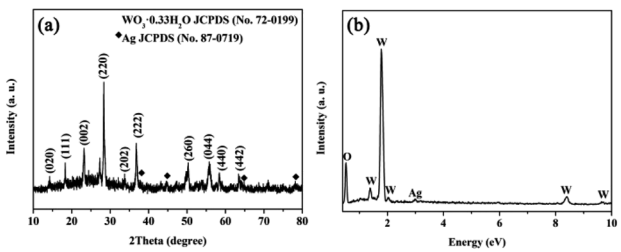

Fig. 1 (a) XRD and (b) EDX of the as-synthesized Ag/$WO_3 \cdot 0.33H_2O$.

[a]*Department of Chemistry, Fudan University, Shanghai 200433, China. E-mail: 13307110326@fudan.edu.cn*

[b]*School of Material Science and Engineering, Xi'an University of Technology, Xi'an 710048, China. E-mail: yangqing@xaut.edu.cn*

† Electronic supplementary information (ESI) available: Experimental section, TGA analysis, XPS spectrum as well as ultraviolet photoemission spectrum of the urchin-like $WO_3 \cdot 0.33H_2O$, and recycled photodegradation performance of the Ag/$WO_3 \cdot 0.33H_2O$ composites. See DOI: 10.1039/c6ra28015c

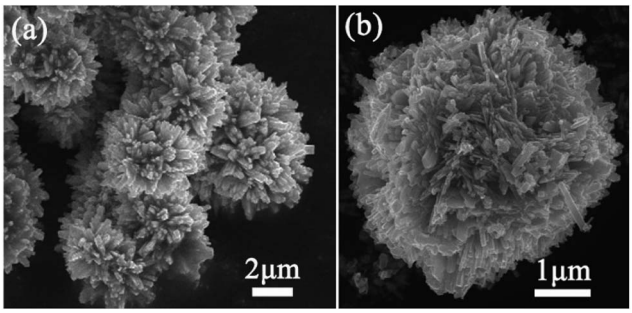

Fig. 2 SEM images of the as-synthesized Ag/$WO_3 \cdot 0.33H_2O$. (a) Low-magnification, (b) high-magnification.

displays that the as-synthesized Ag/$WO_3 \cdot 0.33H_2O$ composite exhibits a three dimensional (3D) urchin-like architectures. A high-magnification SEM image (see Fig. 2b) presents that the hierarchical architecture is assembled by a number of outward radioactive rods-like building blocks with a length of 200–300 nm. Fig. 3a is a typical low-magnification transmission electron microscope (TEM) image of a rod-like building block of the urchin-like Ag/$WO_3 \cdot 0.33H_2O$, and it can be found that some uniform and monodispersed Ag nanoparticles with an average size of 7–9 nm are obviously anchored onto the rod-like $WO_3 \cdot 0.33H_2O$ building block. The detailed microstructures of the rod-like $WO_3 \cdot 0.33H_2O$ building block and Ag nanoparticle

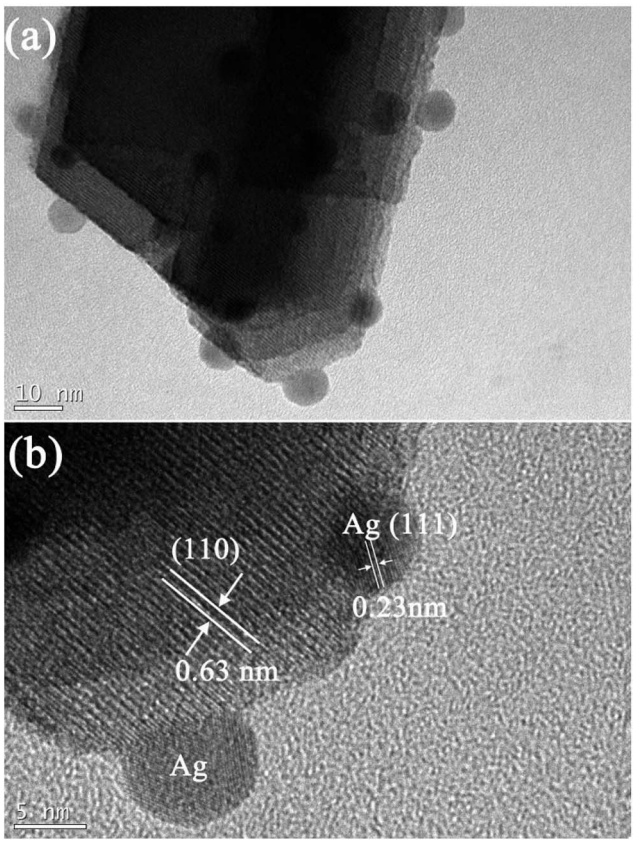

Fig. 3 (a) A typical TEM image of a rod-like building block of the urchin-like Ag/$WO_3 \cdot 0.33H_2O$, (b) the corresponding HRTEM image.

are further investigated by the high resolution transmission electron microscope (HRTEM), as shown in Fig. 3b. The lattice fringes are marked by white lines and arrows. The corresponding lattice spacing of the rod is about 0.63 nm, which is in good agreement with the *d* value of the (110) facet of $WO_3 \cdot 0.33H_2O$ crystal. The lattice spacing of the Ag nanoparticles is about 0.23 nm, which is corresponding to the (111) facet of Ag crystal. Based on the above information, ultrathin Ag nanoparticles anchored on urchin-like $WO_3 \cdot 0.33H_2O$ assemblies is successfully achieved in this work.

The formation of Ag/$WO_3 \cdot 0.33H_2O$ composite is based on a self-catalytic reduction route, which might be attributed to the *in situ* reduction of $AgNO_3$ precursors by the low-valence W^{5+} site in $WO_3 \cdot 0.33H_2O$. The valence state of tungsten element was measured by X-ray photoelectron spectroscopy (XPS, see ESI, Fig. S1†). The peaks at binding energies of 35.3 eV and 37.4 eV correspond to $W4f_{7/2}$ and $W4f_{5/2}$ of W^{6+}, while the peak at binding energy of 36.0 eV corresponds to that of W^{5+}.[13] On account of the fact that the redox pair value of W^{6+}/W^{5+} (+0.26 V, *vs.* SHE) is much lower than that of a redox Ag^+/Ag pair (+0.799 V, *vs.* SHE), the Ag nanoparticles can be reduced in theory. A two-step formation process is proposed as follows, (i) the formation of urchin-like $WO_3 \cdot 0.33H_2O$ precursors by a surfactant-free hydrothermal heating the mixture of tungsten powder/H_2O_2/NaCl, (ii) the preparation of Ag/$WO_3 \cdot 0.33H_2O$ in an aqueous solution at room temperature with a multi-step injection of $AgNO_3$ through an *in situ* redox reaction between weakly reductive W^{5+} sites and oxidative $AgNO_3$ in aqueous solution. Once the Ag^+ ions contacted with the low-valence W^{5+} sites, they would be gradually reduced and *in situ* nucleated on the surface of $WO_3 \cdot 0.33H_2O$, finally leading to the formation of ultrathin Ag nanoparticles by a Ostwald ripening process, which is similar to that occurred in the previous ref. 14 However, in this present work, the morphology and crystalline phase of pristine $WO_3 \cdot 0.33H_2O$ precursors can be saved after depositing Ag nanoparticles.

In order to investigate the change of optical property induced by the introduction of Ag nanoparticles, UV-vis diffuse reflectance measurement was carried out. It can be seen that the absorption edge of the as-synthesized Ag/$WO_3 \cdot 0.33H_2O$ sample displays an obvious red shift compared to the pristine $WO_3 \cdot 0.33H_2O$ (see Fig. 4a), which can be attributed to the localized surface plasmon resonance (LSPR) of Ag nanoparticles.[15] It is noted that the increase of light-harvesting is beneficial to enhance the photocatalytic performance.[16]

The photocatalytic activity of the as-synthesized Ag/$WO_3 \cdot 0.33H_2O$ sample was evaluated by measuring the photodegradation of RhB solution under solar light irradiation. For comparison, the photodegradation activity of the pristine $WO_3 \cdot 0.33H_2O$ without Ag nanoparticles was also carried out. The characteristic absorption peak at 553 nm of RhB was used to monitor the photocatalytic degradation process. A better photocatalytic activity of Ag/$WO_3 \cdot 0.33H_2O$ composite than that of the individual $WO_3 \cdot 0.33H_2O$ can be directly seen in the curves shown in Fig. 4b. The red curve (pristine $WO_3 \cdot 0.33H_2O$) indicated that the photodegradation of RhB decreased rapidly with the extension of exposure time, and about 87% of the RhB

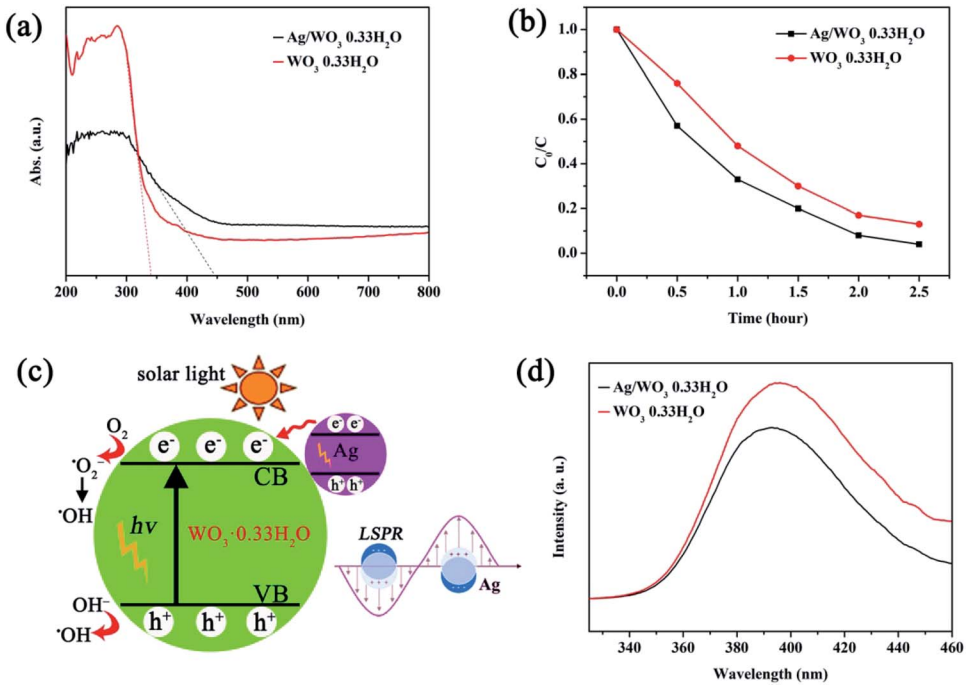

Fig. 4 (a) UV-vis diffuse reflectance spectra of $Ag/WO_3 \cdot 0.33H_2O$ and $WO_3 \cdot 0.33H_2O$, (b) photocatalytic degradation of RhB dye in the presence of $Ag/WO_3 \cdot 0.33H_2O$ and $WO_3 \cdot 0.33H_2O$ under solar light irradiation, (c) a schematic illustration of the synergistic effect between Ag and $WO_3 \cdot 0.33H_2O$, (d) photoluminescence spectra of $Ag/WO_3 \cdot 0.33H_2O$ and $WO_3 \cdot 0.33H_2O$.

was degraded after 2.5 hour. However, it can be found that black curve ($Ag/WO_3 \cdot 0.33H_2O$) decreased further compared to the above red curve, displaying a noticeable photocatalytic degradation of RhB, and about 96% of the RhB was degraded after 2.5 hour. Therefore, the decomposition of the RhB aqueous solution after 2.5 hour in the presence of above two samples is ordered as follows: $Ag/WO_3 \cdot 0.33H_2O$ (96%) > original $WO_3 \cdot 0.33H_2O$ (87%). Fig. S3† shows the recycled experiment of the photodegradation of RhB. It was observed that about 92% of RhB was photodegraded after three successive cycles.

Based on the above photocatalytic results, it is proposed that the as-synthesized $Ag/WO_3 \cdot 0.33H_2O$ composite with a better photodegradation activity can be attributed to the introduction of Ag nanoparticles on the original $WO_3 \cdot 0.33H_2O$ semiconductor, which results in the increase of light-harvesting (see Fig. 4a) and the generation of a synergistic effect between Ag plasmonic photocatalysis and $WO_3 \cdot 0.33H_2O$ semiconductor. The photocatalytic mechanism might be explained as follows. After anchoring Ag nanoparticles onto the urchin-like $WO_3 \cdot 0.33H_2O$, a metal–semiconductor heterojunction would be formed. Since the n type $WO_3 \cdot 0.33H_2O$ semiconductor has a higher work function ($\Phi_{WO_3 \cdot 0.33H_2O} = 5.32$ eV, see Fig. S4, ESI†) than Ag nanoparticle ($\Phi_{Ag} = 4.25$ eV),[17] thus the Fermi level of $WO_3 \cdot 0.33H_2O$ is lower than that of Ag, and the photoexcited electrons would transfer from Ag to $WO_3 \cdot 0.33H_2O$. This phenomenon is similar to the case occurred in a previous report.[17] Under solar light illumination, LSPR-excited electrons would generate and occupy on the surface of Ag owing to their strong LSPR, as demonstrated by Fig. 4a. Besides this LSPR effect, the $WO_3 \cdot 0.33H_2O$ semiconductor would also be directly photoexcited under solar light illumination, thus electrons in the valence band (VB) could excited to the CB, with simultaneous formation of holes in the VB. Combination with the injected LSPR electrons from Ag nanoparticles, the photoexcited electrons in the CB would initiate the photocatalytic reaction. As a result, the interfacial junction between Ag and $WO_3 \cdot 0.33H_2O$ could obviously facilitate the charge separation in LSPR-excited Ag nanoparticles and form long-life charge carriers.[17,18] During the photocatalytic process, these photoexcited electrons could be trapped by the adsorbed O_2 and generate the superoxide anion radicals ($\cdot O_2^-$), which were further reduced to $\cdot OH$ radicals.[19] It has been demonstrated that the $\cdot OH$ radical was in favor of oxidizing organic contaminates owing to its high oxidative capacity.[19] Furthermore, the photoexcited holes might be captured by OH^-, leading to the formation of hydroxyl radical species ($\cdot OH$).[19] A schematic illustration of the synergistic effect between Ag and $WO_3 \cdot 0.33H_2O$ is shown in Fig. 4c. This synergistic effect is proposed to arise from LSPR enhancement on Ag,[17] which could produce more photoexcited electrons in the CB of $WO_3 \cdot 0.33H_2O$ under solar light irradiation, thus suppressing the recombination of electron–hole pairs. Therefore, the photocatalytic activity of $Ag/WO_3 \cdot 0.33H_2O$ would be obviously improved compared to the pristine $WO_3 \cdot 0.33H_2O$.

In principle, an efficient electron–hole separation can strongly suppress the charge recombination, which was confirmed by the photoluminescence (PL) spectrum, because the recombination generally induced luminescence.[11,18] As shown in Fig. 4d, the relatively strong photoluminescence is quenched in the $Ag/WO_3 \cdot 0.33H_2O$ sample, indicating that the

recombination of electron–hole pairs can be more efficiently suppressed, resulting in the enhancement of charge separation. This is agreement with the above photocatalytic result (see Fig. 4b).

In summary, ultrathin Ag nanoparticles anchored on urchin-like $WO_3 \cdot 0.33H_2O$ can be successfully achieved by a novel and facile self-catalytic reduction approach. The as-prepared Ag/$WO_3 \cdot 0.33H_2O$ composite presents a better photodegradation of RhB than that of the individual $WO_3 \cdot 0.33H_2O$ under solar light irradiation, which is attributed to a synergistic effect between Ag plasmonic photocatalysis and $WO_3 \cdot 0.33H_2O$ semiconductor. The synergistic effect is thought to arise from LSPR enhancement on Ag, which produces more photoexcited electrons in the CB of $WO_3 \cdot 0.33H_2O$ under solar light irradiation, suppressing the recombination of electron–hole pairs. The results provide a convincing evidence for the designate synthesis of metal–semiconductor heterojunction with improved functionality.

Acknowledgements

Haoqi Ren deeply appreciates Prof. Hong Yang offered the chance of summer internship at University of Illinois at Urbana-Champaign, and thanks Prof. Yang and Mr Kai-Chieh Tsao for the useful discussion and suggestions for this work. This work was financially supported by the innovation funds from youth league committee in Fudan University, and the National Science Foundation of China (NSFC No. 51471132).

Notes and references

1 M. D'Arienzo, L. Armelao, C. M. Mari, S. Polizzi, R. Ruffo, R. Scotti and F. Morazzoni, *J. Am. Chem. Soc.*, 2011, **133**, 5296–5304.
2 X. He, C. Hu, Q. Yi, X. Wang, H. Hua and X. Li, *Catal. Lett.*, 2012, **142**, 637–645.
3 J. C. Shi, G. J. Hu, R. Cong, H. J. Bu and N. Dai, *New J. Chem.*, 2013, **37**, 1538–1544.
4 X. Y. He, C. G. Hu, Q. N. Yi, X. Wang, H. Hua and X. Y. Li, *Catal. Lett.*, 2012, **142**, 637–645.
5 B. X. Liu, J. S. Wang, J. S. Wu, H. Y. Li, H. Wang, Z. F. Li, M. L. Zhou and T. Y. Zuo, *Mater. Lett.*, 2013, **91**, 334–337.
6 X. Q. Gao, C. Yang, F. Xiao, Y. Zhu, J. D. Wang and X. T. Su, *Mater. Lett.*, 2012, **84**, 151–153.
7 J. Y. Li, J. F. Huang, J. P. Wu, L. Y. Cao, Q. J. Li and K. Yanagisawa, *CrystEngComm*, 2013, **15**, 7904–7913.
8 Y. Zheng, G. Chen, Y. G. Yu, J. X. Sun, Y. S. Zhou and J. Pei, *CrystEngComm*, 2014, **16**, 6107–6113.
9 M. S. Bazarjani, M. Hojamberdiev, K. Morita, G. Zhu, G. Cherkashinin, C. Fasel, T. Herrmann, H. Breitzke, A. Gurlo and R. Riedel, *J. Am. Chem. Soc.*, 2013, **135**, 4467–4475.
10 F. Wang, C. D. Valentin and G. Pacchioni, *J. Phys. Chem. C*, 2012, **116**, 10672–10679.
11 Y. Zheng, G. Chen, Y. G. Yu, Y. Zhou and F. He, *Appl. Surf. Sci.*, 2016, **362**, 182–190.
12 X. Y. He, C. G. Hu, Y. Xi, K. Y. Zhang and H. Hua, *Mater. Res. Bull.*, 2014, **5**, 91–94.
13 C. Lian, X. L. Xiao, Z. Chen, Y. X. Liu, E. Y. Zhao, D. S. Wang, C. Chen and Y. D. Li, *Nano Res.*, 2016, **9**, 435–441.
14 G. C. Xi, J. H. Ye, Q. Ma, N. Su, H. Bai and C. Wang, *J. Am. Chem. Soc.*, 2012, **134**, 6508–6511.
15 S. K. Cushing, J. T. Li, F. K. Meng, T. R. Senty, S. Suri, M. J. Zhi, M. Li, A. D. Bristow and N. Q. Wu, *J. Am. Chem. Soc.*, 2012, **134**, 15033–15041.
16 X. M. Zhang, Y. L. Chen, R. S. Liu and D. P. Tsai, *Rep. Prog. Phys.*, 2013, **76**, 046401.
17 J. Jiang, H. Li and L. Z. Zhang, *Chem.–Eur. J.*, 2012, **18**, 6360–6369.
18 S. Bai, J. Jiang, Q. Zhang and Y. J. Xiong, *Chem. Soc. Rev.*, 2015, **44**, 2893–2939.
19 Q. Xiang, G. F. Meng, H. B. Zhao, Y. Zhang, H. Li, W. J. Ma and J. Q. Xu, *J. Phys. Chem. C*, 2010, **114**, 2049–2055.

